THE JOURNAL OF PHYSICAL CHEMISTRY B
A JOURNAL OF THE AMERICAN CHEMICAL SOCIETY

pubs.acs.org/JPCB

Article

Modeling the Mechanical Response of Microtubule Lattices to Pressure

Published as part of The Journal of Physical Chemistry virtual special issue "Dave Thirumalai Festschrift".

Lukasz Szatkowski, Rohith Anand Varikoti, and Ruxandra I. Dima*

Cite This: https://doi.org/10.1021/acs.jpcb.1c01770

Read Online

ACCESS | Metrics & More | Article Recommendations | Supporting Information

ABSTRACT: Microtubules, the largest and stiffest filaments of the cytoskeleton, have to be well adapted to the high levels of crowdedness in cells to perform their multitude of functions. Furthermore, fundamental processes that involve microtubules, such as the maintenance of the cellular shape and cellular motion, are known to be highly dependent on external pressure. In light of the importance of pressure for the functioning of microtubules, numerous studies interrogated the response of these cytoskeletal filaments to osmotic pressure, resulting from crowding by osmolytes, such as poly(ethylene glycol)/poly(ethylene oxide) (PEG/PEO) molecules, or to direct applied pressure. The interpretation of experiments is usually based on the assumptions that PEG molecules have unfavorable interactions with the microtubule lattices and that the behavior of microtubules under pressure can be described by using continuous models. We probed directly these two assumptions. First, we characterized the interaction between the main interfaces in a microtubule filament and PEG molecules of various sizes using a combination of docking and molecular dynamics simulations. Second, we studied the response of a microtubule filament to compression using a coarse-grained model that allows for the breaking of lattice interfaces. Our results show that medium length PEG molecules do not alter the energetics of the lateral interfaces in microtubules but rather target and can penetrate into the voids between tubulin monomers at these interfaces, which can lead to a rapid loss of lateral interfaces under pressure. Compression of a microtubule under conditions corresponding to high osmotic pressure results in the formation of the deformed phase found in experiments. Our simulations show that the breaking of lateral interfaces, rather than the buckling of the filament inferred from the continuous models, accounts for the deformation.

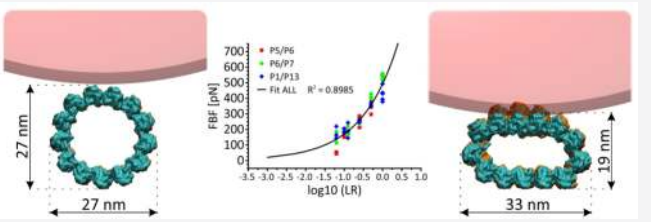

INTRODUCTION

Cells are highly crowded environments for biomolecules, where the density of macromolecules can be as high as 500 g/L.[1] Microtubules (MTs), which are the largest and stiffest filament of the cytoskeleton, need to be well tuned to this high degree of crowdedness to carry their multiple cellular functions. Indeed, experiments pointed to the adaptation of the function of transport of cargoes along MTs when kinesins are crowded around MT filaments.[2] Furthermore, the crowded cellular environment, where up to 40% of the cellular volume is occupied by various macromolecules, can result in depletion attraction: the ensuing effect of excluded volume increases the osmotic pressure and entropy penalty, leading to attractive forces between MTs.[3] Finally, tasks such as maintenance of the cellular shape, cellular motion, and mechanical strength, which are all intimately dependent on the dynamics of the cytoskeleton, are among the most pressure-sensitive processes found *in vivo*.[3]

In view of the importance of MT adaptation to crowdedness and high pressure for functional purposes, it is crucial to determine how different is the behavior of MTs under various regimes of pressure. MTs are polymeric assemblies of α- and β-tubulin dimers longitudinally connected to each other by noncovalent bonds into long protofilaments. The size of a tubulin dimer is ∼8 nm, with MTs reaching micrometers to millimeters in length. The standard form of MTs in cells is a hollow cylinder composed of 13 such protofilaments connected by lateral bonds, which consist primarily of contacts between charged residues. The outer diameter of the MT is ∼27 nm, and the inner diameter is ∼18 nm. While most of the lateral bonds are between the same type monomers (homotypic), i.e., $\alpha-\alpha$ and $\beta-\beta$, corresponding to a B-lattice arrangement, the 13-protofilament MT has one special lateral interface called the seam, which consists of contacts between $\beta-\beta$ monomers (heterotypic) or an A-lattice, between protofilaments 1 and 13. Moreover, at the seam there is a

Received: February 26, 2021
Revised: April 26, 2021

shift of three monomers between the adjacent protofilaments resulting in a helical rather than cylindrical overall structure for the MT filament. Recent experimental studies investigated the effect of crowding by osmolytes such as poly(ethylene oxide)/(poly(ethylene glycol) (PEO/PEG) or of the corresponding osmotic pressure[4−8] and of applied high pressure on MTs.[3] The main findings are the following: (1) Osmotic pressure starting from ∼600 Pa, corresponding to a 1% w/v PEO20k solution, drives the assembly of MTs into ordered rectangular bundles. Of note, MTs in these bundles are no longer circular but rather elliptical in cross section.[4,5] The authors attributed the change in cross section to the buckling of MTs. Moreover, they showed that this process is reversible: if the MTs in this phase are sedimented by centrifugation and resuspended in a buffer without PEO, they become unbundled and form a nematic phase of unbuckled, undamaged MTs. (2) Under a high pressure of 155 MPa active MTs (without taxol) disintegrate into protofilaments due to the breaking of the lateral contacts that connect protofilaments in the MT lattice.[3] (3) In the presence of 10 and 20 wt % PEG 20k MTs form bundles,[3−5] which are more resistant to pressure-induced dissociation compared to single MTs: they remain intact until the applied pressure exceeds 190 MPa, an ∼20% increase in stability versus single MTs.[3] (4) The measurement of the depletion interaction between a pair of MT filaments, using a combination of single filament imaging and optical trapping,[7] showed that the degree of attractive interaction between MTs increases with both the level of crowding (by PEG) and the salt (K^+) concentration as MTs have a high negative charge density on their outer surface due to the charged and disordered C-terminal tails (CTTs) of the tubulin monomers. (5) PEG does not interact with the CTTs.[8] (6) The 25% w/v solutions of large molecules (PEG600 and PEG10k) stabilize MTs against depolymerization at room temperature over a 24 h period. These authors also found that the presence of PEG10K induced MT bundling.[8] Interestingly, they did not find evidence of 25% w/v PEG600 diffusing into the lumen of MTs even after a week of exposure, in contrast with earlier experiments.[4,5]

The interpretation of the effect that crowding by osmolytes such as PEO/PEG and of pressure (osmotic or directly applied pressure) has on MTs in experiments was often based on continuous models that represented a MT either as a vesicle (free[9] or confined to a wall[10]) or as a shell (isotropic or anisotropic[7,11]). Such an elastic shell model, which accounts for the anisotropy of a MT filament, was further used for example to describe the softening of the cross section of MT lattices upon application of mechanical forces in LOT experiments.[11] These models, while being able to characterize the curvature of a MT due to buckling, do not allow for the probing of any pressure-induced breaking in the MT lattice such as the formation of cracks and their propagation. Moreover, while it has been shown that the interaction between PEGs and tubulin subunits is unfavorable,[5] no direct investigation into the nature of PEGs interaction with MTs exists. This is an important problem as recent reports showed that PEG molecules in bulk can interact with proteins and change their conformation and electrostatics.[12−15] Thus, there is a need for computational/theoretical models, which can provide an in-depth look at the nature of the interactions between PEGs and MT surfaces and at the mechanical response of MTs under high crowdedness or pressure. Previously, we employed a coarse-grained atomistic modeling of a full MT lattice with 13 protofilaments, which enabled us to shed light on the molecular-level structural changes and breaking patterns that account for the behavior of MTs during AFM indentation experiments[16,17] or during *in vitro* severing.[18,19] In these studies we modeled the mechanical response of MTs of varying lengths, with either one or both ends fixed, to concentrated forces applied under constant loading rates from the AFM regime on the outer surface of the lattice to mimic the corresponding experimental conditions.[20,21]

The goal of this paper is twofold. First, we directly test the nature and extent of interactions between the main types of lateral interfaces in an MT filament and PEG molecules of varying molecular weights using a combination of docking and atomistic molecular dynamics (MD) simulations. In these studies, we used short to medium length PEG molecules (from 5 to 75 monomers), not only for making the computations more tractable but also because shorter PEGs diffuse faster than longer chains and thus allow for a fast sampling of the modes of interaction with the MT surfaces. In addition, many experiments have been performed in the presence of both shorter and longer length PEGs.[4,5,8] Moreover, as the persistence length of PEG molecules is comparable to the distance between monomers (0.38 nm),[22] the medium length PEGs used in our simulations should be able to capture the flexibility of the longer PEGs used in experiments, resulting in similar binding positions on the surface of MTs. Second, starting from our previous work and the results of the analysis of the PEG−MT interactions, we determine the mechanical response of a 13-protofilament MT with both ends free under conditions mimicking low and high crowdedness, while employing a model that allows for lattice contacts breaking.[23] Importantly, unlike our past work, here we apply forces to the MT filament under ever decreasing loading rate conditions, which allows us to extrapolate our results to the vanishingly low rates corresponding to the above experiments. Our main findings are that medium length PEG molecules do not influence the energetics of lateral interfaces in MT filaments, primarily because they target voids or packing defects at these interfaces. This behavior, coupled with Le Chatelier's principle, helps explain why lateral interfaces are the first surfaces to break under high concentration of PEGs. Second, our coarse-grained simulations of the compression of MTs predict that the first breaking event, which is the loss of lateral interfaces, corresponds to the same pressure regime and has the same structural signature as in studies of crowding of MTs by long PEG molecules.[3−5] Because lateral interface breaking is reversible, our results provide a microscopic interpretation for such experiments.

METHODS

Interactions between Microtubules (MTs) and Poly(ethylene glycol) (PEG). *Docking Studies.* For docking PEG molecules onto a 13-protofilament MT, we considered fragments representative for the two different types of lattices (A and B) of a MT: the seam interface (SEAM, between protofilaments P1/P13) and the regular lateral (away from the seam) interface (AWAY, between protofilaments P6/P7). We started from the equilibrated full atomistic structure of the 13-protofilament MT with 8 dimers length, which we used to construct our coarse-grained SOP model.[17] Because this structure contains ∼1.4 million atoms, which is too big for docking, we selected smaller fragments corresponding to the regions of interest (SEAM and AWAY): 2 × 4 matrices (2

https://doi.org/10.1021/acs.jpcb.1c01770
J. Phys. Chem. B XXXX, XXX, XXX−XXX

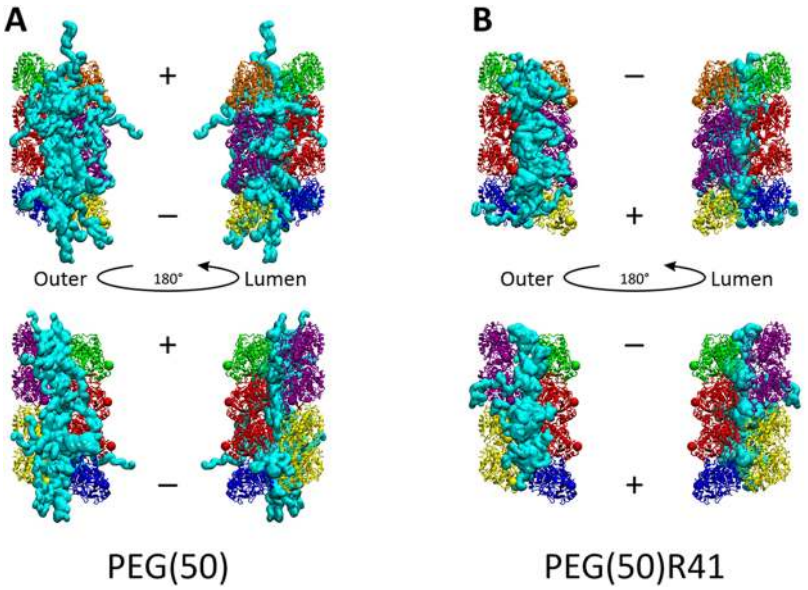

Figure 1. Comparison of docking results for PEG molecules, with a mass of 2000 Da (50 monomers long), in the state with the longest end-to-end distance (81 Å; panel A; PEG(50)) and the state corresponding to the most probable end-to-end distance (41 Å; panel B; PEG(50)R41) onto the AWAY (top row) and SEAM (bottom row) MT interfaces (colors are the same as in Figure S1). The + and − ends of the MT are labeled. Cyan surfaces represent an overlap of the 50 positions for PEG(50) or PEG(50)R41 corresponding to the lowest energy form each of three independent docking runs. Spheres represent the C-terminus amino acid of each monomer. Left panels: view from the outer surface of the MT. Right panels: view from the lumen of the MT.

protofilaments, 4 monomers in length in each protofilament) such that in the middle of the matrices we have a full tubulin dimer, which interacts laterally with tubulin monomers from the other protofilament ($\beta\alpha\beta\alpha$:$\beta\alpha\beta\alpha$ for the AWAY model and $\beta\alpha\beta\alpha$:$\alpha\beta\alpha\beta$ for the SEAM model; see Figures S1 and S2 in the Supporting Information).

In view of the variety of PEG lengths used in experiments, we selected for docking PEG molecules with the following masses: 200 Da (5 monomers, PEG(5)), 400 Da (10 monomers, PEG(10)), 600 Da (15 monomers, PEG(15)), 800 Da (20 monomers, PEG(20)), 1000 Da (25 monomers, PEG(25)), 1200 Da (30 monomers, PEG(30)), 1400 Da (35 monomers, PEG(35)), 1600 Da (40 monomers, PEG(40)), 1800 Da (45 monomers, PEG(45)), 2000 Da (50 monomers, PEG(50)), 2200 Da (55 monomers, PEG(55)), 2400 Da (60 monomers, PEG(60)), 2600 Da (65 monomers, PEG(65)), 2800 Da (70 monomers, PEG(70)), and 3000 Da (75 monomers, PEG(75)). Employing PEGs with higher masses becomes prohibitive for docking. To determine the structure of each PEG molecule to be used for docking, each PEG was minimized (for 2500 steps), heated (from 0 to 300 K by using a temperature increment of 1 K/1000 steps and 10000 additional steps to be sure that the temperature is stable), and equilibrated for 5 ns (1 ns per 1000000 steps) by using the NAMD 2.2 software with the CHARMM 27 force field and the Generalized Bohr Continuum Solvent model.[24,25] Finally, we selected for each PEG molecule the structure corresponding to the longest value of the end-to-end distance from the last 2 ns of the equilibration. We made this choice to probe the maximal effect that PEGs have on the MT lattice. In view of the proposal that medium length PEGs are likely to induce changes in protein structures,[12] we also performed docking studies using the structure of PEG2000 corresponding to its most probable end-to-end distance value. Operationally, we selected from our initial equilibration run the structure of a PEG molecule with 50 monomers (PEG(50)) and an end-to-end distance equal 41 Å (called PEG(50)R41), which matches the recently measured most probable value for PEG(50) in water.[26]

To dock PEG molecules onto the MT fragments, we used the BUDE software.[27] The first step was the generation of receptor grid points around both the SEAM and AWAY models. Because we used only fragments from a MT lattice and the BUDE software does not allow for the selection of only a region of the system where receptor grid points would be generated, we deleted all the generated grid points corresponding to the MT lumen and to the lateral/longitudinal interfaces that in a full MT structure would be in contact with the adjacent tubulin monomers, thus leaving only the points that would be located on the outer surface of the filament. That reduced the total number of receptor grid points from 82000 to 22000. Next, we used BUDE to create three surface files with randomly selected 9999 surface grid points for each system (SEAM and AWAY), which we used for docking (see Figure S3).

From each MT PEG docking run, we selected 200 poses of PEGs with the lowest energy to visually evaluate whether a PEG molecule binds on the dimer surfaces, on the lateral, or on the longitudinal interfaces of an MT. Additionally, we combined the first 50 poses (with the lowest energy) from each of the three separate docking runs (for the 9999 randomly selected grid points each) and used them to create a density map of PEG molecules around MTs.

Molecular Dynamics Simulations of the PEG−MT Complexes. Because the highest density of PEG(50) molecules from docking was along the lateral interfaces (Figure 1), and these interfaces are the first to break under high pressure,[3] we studied the influence of PEG molecules on these interfaces between protofilaments in a MT filament. Here we performed atomistic MD simulations in explicit solvent. For our studies we selected PEG(50) molecules because they are among the category of PEGs most likely to

https://doi.org/10.1021/acs.jpcb.1c01770
J. Phys. Chem. B XXXX, XXX, XXX−XXX

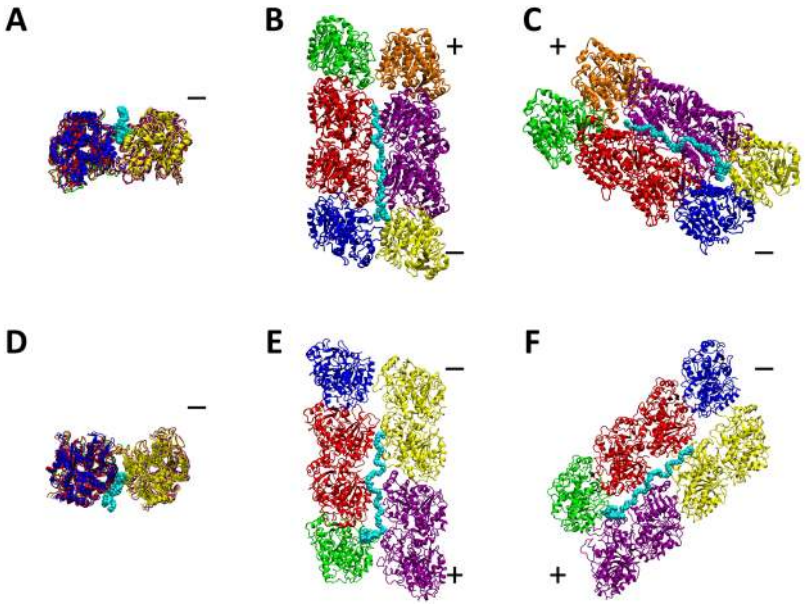

Figure 2. Selected poses for a PEG(50) molecule (with 50 monomers as cyan spheres) for full atomistic MD studies. View from the + side (A: AWAY; D: SEAM), from the top (B: AWAY; E: SEAM), and from an angle (C: AWAY; F: SEAM). Full dimers have the same colors; the + and − ends of the MT fragments are indicated.

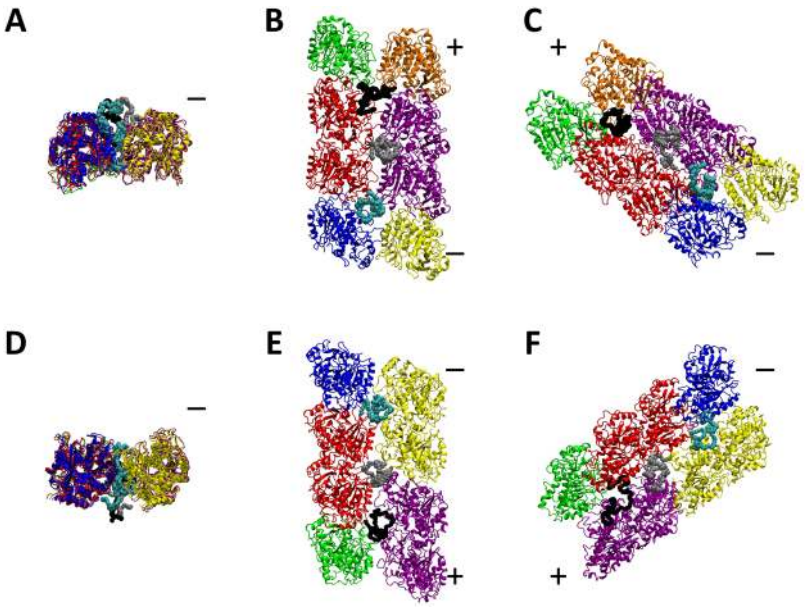

Figure 3. Selected poses for a PEG(50)R41 molecule (with 50 monomers as cyan, silver, and black spheres) for full atomistic MD studies. View from the + side (A: AWAY; D: SEAM), from the top (B: AWAY; E: SEAM), and from an angle (C: AWAY; F: SEAM). Full dimers have the same colors; the + and − ends of the MT fragments are indicated.

induce changes in protein structures[12] and because the largest value of their end-to-end distance is ∼8 nm, which is commensurate with the length of a tubulin dimer. To determine the starting structure, we selected, for each MT model (SEAM and AWAY), the PEG(50) docking poses that visually fit along the entire lateral interface between the middle full tubulin dimer and the corresponding tubulin subunit from the next protofilament in the SEAM and the AWAY model, respectively (Figure 2 and Figures S1 and S2). We used a similar approach to prepare the starting structures of the AWAY and SEAM models with PEG(50)R41. However, because PEG(50)R41 is substantially more compact than PEG(50), to examine MT structures with similar coverage of lateral interfaces for both types of PEG2000 structures, this time we started from the docked configurations with three PEG(50)R41 molecules for each system (see Figure 3). Next, by using VMD,[28] we fully solvated the systems in water employing a box of size 20 Å from the surface of the MT matrices, and we added Na^+ and Cl^- ions to neutralize the system and create a solution with 0.15 M ionic strength. Finally, to mimic the fact that the fragment is in fact a part of a full MT filament (with 13 PFs), we froze 252 Cα atoms from the outer edge of the 2 × 4 MT matrices (Figure S4), while leaving it enough internal freedom to adapt to the presence of PEGs. To map out the differences due to the presence of PEG, we also simulated the two reference systems (for AWAY and

https://doi.org/10.1021/acs.jpcb.1c01770
J. Phys. Chem. B XXXX, XXX, XXX−XXX

SEAM) without the PEGs. All systems have comparable sizes of ~360000 atoms (see Table S1 for details about the system size and number of trajectories).

We used the NAMD package[25] with the CHARMM27 force field, periodic boundary conditions, particle mesh Ewald electrostatics, and the Shake algorithm to perform the MD simulations for each system. We started by minimizing the system for 2500 steps and then heating for 300000 steps from 0 to 300 K (with a temperature increase of 1 K/1000 steps) and an additional 10000 steps to be sure that the temperature is stable. During equilibration, we used the Langevin piston and Langevin thermostat to keep the system at 1 atm and 300 K. Following the equilibration run for 1690000 steps (up to 2 ns together with heating), we performed 20 ns production runs.

Analysis of the MD Simulations. For each production run, we calculated the root-mean-square deviation (RMSD; see Figures S5 and S6) of the backbone atoms in the MT system (MT for reference systems; MT and PEG for the system with the PEG(50)/PEG(50)R41 molecule(s)) versus the structure from the last step of the equilibration. The last 2 ns from each production run was selected for energy analysis (the electrostatic (Coulombic), van der Waals, and nonbonded energy; see Figure S7) to determine if PEG2000 molecules influence the energetics of lateral interactions in MTs for the AWAY and SEAM interfaces. We also performed an analysis of the interactions between the central dimer and corresponding adjacent tubulin monomers (see Figure S2) to evaluate the effect of PEGs on the monomer−monomer interactions at the lateral interfaces in a MT. Finally, we calculated the change of the position of PEG molecules with respect to the lateral interface and the number of water molecules at the lateral interface. Details are provided in section I.1 of the Supporting Information.

MT Compression Studies. *Setup and Dynamics of Coarse-Grained Simulations.* For the MT filament indentation (compression) studies we used the self-organized polymer (SOP) model with Brownian dynamics[23] implemented on graphics processing units[29] called gSOP (ver. 1.07 and 2.0). The covalent bonds were described through the finite extensible nonlinear elastic potential (V_{FENE}), while for the native noncovalent interactions we used the full Lennard-Jones potential ($V_{\mathrm{NB}}^{\mathrm{ATT}}$). Additionally, all the non-native, nonbonded interactions ($V_{\mathrm{NB}}^{\mathrm{REP}}$) were described by using only the repulsive part of the Lennard-Jones potential. Therefore, the total energy of the polymer in the SOP model can be calculated from the following equations:

$$V_{\mathrm{T}} = V_{\mathrm{FENE}} + V_{\mathrm{NB}}^{\mathrm{ATT}} + V_{\mathrm{NB}}^{\mathrm{REP}} \tag{1}$$

$$V_{\mathrm{FENE}} = \sum_{i=1}^{N-1} \frac{k}{2} {R_0}^2 \log\left(1 - \frac{(r_{i,i+1} - r_{i,i+1}^0)^2}{{R_0}^2}\right) \tag{2}$$

$$V_{\mathrm{NB}}^{\mathrm{ATT}} = \sum_{i=1}^{N-3} \sum_{j=i+3}^{N} \epsilon_{\mathrm{h}} \left[\left(\frac{r_{ij}^0}{r_{ij}}\right)^{12} - 2\left(\frac{r_0^{ij}}{r_{ij}}\right)^6\right] \Delta_{ij} \tag{3}$$

$$V_{\mathrm{NB}}^{\mathrm{REP}} = \sum_{i=1}^{N-2} \epsilon_l \left(\frac{\sigma_{1,i+2}}{r_{i,i+2}}\right)^6 + \sum_{i=1}^{N-3} \sum_{j=i+3}^{N} \epsilon_l \left(\frac{\sigma}{r_{ij}}\right)^6 \times (1 - \Delta_{ij}) \tag{4}$$

where the strength of the native contacts in the lattice is represented by the ϵ_{h} parameter, which is the only parameter in the preceding equations that can change based on the topology of the system and the type of the contacts in the system. Additionally, the following parameters were introduced into the potential function: the spring constant k = 20.0 kcal/(mol Å^2), the tolerance in distance change for covalent bonds R_0 = 2.0 Å, and the length of the amino acid−amide bond (covalent bond) r_i = 3.8 Å, for i = 1, 2, ..., N, where N is the number of the Nth residue. Finally, the r_{ij} parameters represent the distance between two residues (i and j) in the current structure, while the corresponding r_{ij}^0 is the value in the native structure. Furthermore, two residues i and j (where $|i - j| > 2$), in the nonbonded part of the potential, are considered to be in contact if their Cα atoms were within the cutoff of R_c = 8.0 Å from each other (within the cutoff radius Δ_{ij} = 1 and above Δ_{ij} = 0). Therefore, we generated the initial contact topologies for an input structure with the contact cutoff equal to 8.0 Å criterion for the position of Cα corresponding to each amino acid. The remaining two parameters used in the potential equation were σ = 3.8 Å and l = 1 kcal/mol.

The strength of the native interactions (ϵ_{h}) in the attractive part of the Lennard-Jones potentials was 1.9 kcal/mol for all intradimer interactions (inside the monomer and between two monomers of the same dimer). The potential well depth of the longitudinal interactions (between two dimers) was 1.0 and 0.9 kcal/mol for all lateral interactions and the SEAM interface. These follow the parametrization for the 13-protofilament MT from our previous studies.[16,17] Our model for a MT filament does not include the highly charged and disordered C-terminal tails (CTTs) of the tubulin monomers, thus mimicking a filament resulting from the treatment of MTs with the enzyme subtilisin. We have made this choice as experiments[8] showed that PEGs do not interact with the CTTs.

For indentation we used rigid sphere cantilever tips with various radii, as depicted in Figure 4. Operationally, we

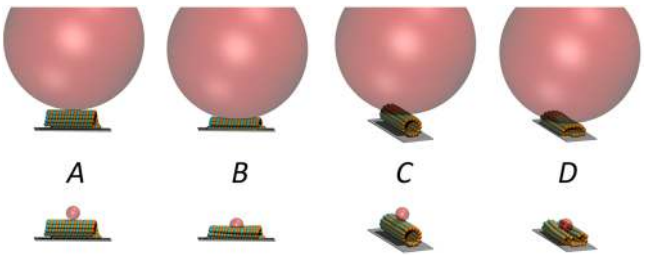

Figure 4. Comparison of two setups for 13-protofilament MT with 8 dimers length, pushing between P6/P7: Big Tip (BT, 100 nm radius tip, top plots) and Small Tip (ST, 10 nm radius tip, bottom plots). View from the side (A) and from the top (C) at the start of trajectory and at the end of the trajectory from the side (B) and from the top (D); orange/cyan spheres are representations of α/β-tubulin monomers; gray spheres the plate, and red sphere the indentation tip.

modified the 13-protofilament MTs (13MTs) indentation protocol from our previous work[17,18] to investigate the behavior of MTs under high crowdedness/pressure by using three different tip sizes: 10 nm (small-sized tip, which is similar to the diameter of the spastin or katanin hexamers.[30] and is the same one used in our previous studies, ST), 75 nm (large-sized tip, LT), and 100 nm (big-sized tip, BT). Additionally, we introduced a set of frozen beads below the MT, called the plate (gray spheres in Figure 4), which can be a mimic of the

https://doi.org/10.1021/acs.jpcb.1c01770
J. Phys. Chem. B XXXX, XXX, XXX−XXX

interaction of one MT filament with neighboring MTs in MT bundles. The interactions between the tip/plate and the MT filament were modeled with the use of the repulsion term of the Lennard-Jones potential, $V_{LJ} = \epsilon_{LJ}(\sigma_{LJ}/(r_i - R_{tip}))^6$, where ϵ_{LJ} = 4.18 kJ/mol, the distance between the center of the tip sphere and the amino acid is σ_{LJ} = 1.0 Å, the position of the ith Cα is described by the parameter r_i, and the tip radius is R_{tip}. The strength of the cantilever spring constant is K_s = 50 pN/nm, following AFM experiments.[20] The movement of the tip was toward the MT surface and perpendicular to the long axis of the MT cylinder. In contrast to our previous work,[16−18] here both ends of the MT were free.

To probe the influence of finite-size effects in our simulations, we used MTs with three different filament lengths (given length is the number of dimers per protofilament): 6 dimers or 51 nm in length, 8 dimers or 68 nm in length, and 12 dimers long or 102 nm in length. Furthermore, we used the following combinations of MTs length and large tip sizes (the number after x is the length of the filament): 13MTx8 with BT, 13MTx12 with BT, and 13MTx6 with LT (this is a similar tip size to MT length ratio like for 13MTx8 with BT) and BT. These combinations of the size of the enlarged tip (LT or BT) and the size of the 13MT filament result in a relatively flat contact area between the tip and the MT, allowing us to carry out simulations that mimic the compression of a MT lattice between two surfaces.

To estimate the range of the force response of the MT network upon external stress, we performed our studies using six different indentation loading rates of decreasing magnitude: 2.000 μm/s (normal loading rate, which is the one used in our previous indentation studies and it is similar to the indentation speed in the AMF experiments[20]), 1.000 μm/s (1/2 of the normal loading rate), 0.500 μm/s (1/4), 0.250 μm/s (1/8), 0.200 μm/s (1/10), and 0.125 μm/s (1/16). Similar to our previous studies, we performed the indentation with the BT on the SEAM interface (the tip was placed above and between the 1st and 13th protofilaments; P1/P13)[18] and opposite to the SEAM interface: directly opposite to the seam, P6/P7, and on the weakest lateral interface in the microtubule, P5/P6.[17] We used Brownian dynamics simulations at 300 K to perform multiple trajectories for each loading rate for each system (see Table S2). The integration time step was 40 ps, which corresponds to a unitless friction coefficient for a residue in water ζ = 50.0. The origin of this time step was described in our previous work[17] and came from $h = 0.16\tau_h$ (where $\tau_h = \frac{\zeta\epsilon_h}{K_B T}\tau_L$ and τ_L = 2.0 ps). Therefore, a frame in our plots corresponds to 40 μs.

Analysis of MT Compression Simulations. The analysis of our simulations consisted in the evaluation of the number of relative native contacts, called RQn (see details in section I.2 of the Supporting Information),[18,19] for each system to find the first breaking force (FBF), which is the force at which the first break occurs in the MT lattice, as well as the corresponding applied pressure. We plotted the FBF versus the log of the relative loading rate (1, 1/2, ..., 1/16) and used OriginPro software to fit the resulting data. By extending the resulting fit to the very low loading rate regime corresponding to *in vitro* experiments, we extracted the minimal force that elicits a mechanical response from a MT filament. We also determined the breaking pathways.

RESULTS AND DISCUSSION

Nature of the Interaction between MTs and PEG. *Docking of PEG Molecules on MT Fragments Shows That PEG Populates Primarily Interfaces with Large Defects/Cavities.* The distributions of the end-to-end distances for the equilibrated PEG molecules from our MD GBSW simulations, shown in Figure S8, agree with the latest experimental and computational data from explicit solvent MD simulations.[26] Thus, the use of the implicit solvent model and the 5 ns long dynamics are sufficient to recreate the correct population of PEG molecules in water. We used the scaling of the end-to-end distance with the molecular weight of the polymer,[26] R_{ee} = 0.047 (nm) × $(MW)^{0.588}$, to find the most probable end-to-end distance for a PEG molecule with molecular weight MW. This corresponds to a semiflexible chain in good solvent, resulting in a similar scaling[31] for the radius of gyration, R_g = 0.0215 (nm) × $(MW)^{0.583}$.

As described in the Methods section, we used the BUDE software to perform the docking of these equilibrated PEGs, ranging in length from 5 to 30 monomers, in the state corresponding to their longest end-to-end distance to the two main fragments from a MT lattice: the SEAM and AWAY models. The analysis of the 200 lowest energy poses for PEGs from the three separate docking runs for each model revealed that the smallest PEG molecule (five monomers long) has equal preference for the lateral and the longitudinal interfaces in both the SEAM and AWAY models (see Figure S9A). For PEGs of increasing chain length, we saw an accumulation primarily along the lateral interfaces (for the 10−35 monomers long PEGs as seen in Figure S9B−G), followed by an increase in density on the surface of the MT (for the 40−75 monomers long PEGs, as seen in Figure S9H−N and Figure 1). In addition, starting from a length of 30 monomers, more PEGs were placed on the edge of the MT fragment, corresponding to configurations where a part of the PEG molecule is sticking outside of the lattice (at the +/− ends of the fragment, above and below). This result recalls the experimental findings regarding the location of the PEG chains of P5K2 on hemoglobin (Hb).[32] Moreover, our finding that PEGs with higher molecular mass were more crowded on the surface of the MT fragment for both the SEAM and AWAY models is consistent with experimental results.[3,8] Analysis of the docking poses for the PEG(50)R41 molecules, with the end-to-end distance of 41 Å matching the most probable state of a PEG molecule with 50 monomers[26] and a radius of gyration of 15.8 Å, showed that it occupies primarily cavities between monomers: it is located at the interface between four monomers originating from either two or four different dimers in both the SEAM and AWAY models (panel B in Figure 1). This finding recalls the data regarding the interaction between hemoglobin (Hb) and PEG chains, as both experiments[32] and simulations of Hb in the presence of PEG5000[33] showed that PEGs occupy the internal cavities between the Hb monomers. In summary, our docking studies showed that irrespective of their end-to-end state, PEG(50)s tend to accumulate at the lateral interfaces between protofilaments in a 13MT lattice, especially near cavities.

Our finding that the nature of the interaction between PEG molecules and MT fragments depends on the molecular weight of the PEGs agrees with results from experimental studies of the interaction between two model proteins (bovine serum albumin and lysozyme) and PEGs of varying MW values.[12]

https://doi.org/10.1021/acs.jpcb.1c01770
J. Phys. Chem. B XXXX, XXX, XXX−XXX

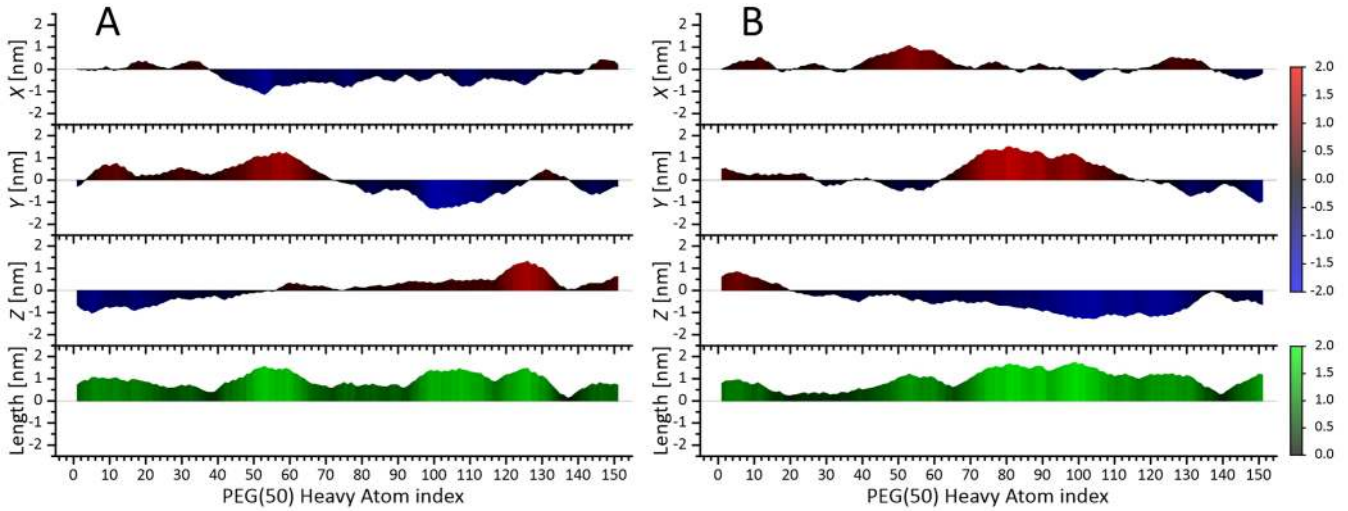

Figure 5. Change in the position of the heavy atoms of PEG(50) in the AWAY+PEG(50) model (panel A) and the SEAM+PEG(50) model (panel B) calculated as the difference between the position in the average structure (from the last 2 ns of the production run) and the initial PEG(50) position after docking. Panels from top to bottom: displacement on the *X*-, *Y*-, and *Z*-axes, and amplitude of displacement. Gradient color codes are on the right panel (top for displacement on the *X*-, *Y*-, and *Z*-axes and bottom for the total length of the displacement vector). The positive change in displacement on the *X*-axis indicates a shift of the position of an atom away from a dimer (toward adjacent tubulin monomers: α46 and β46 for AWAY+PEG(50) and β52 and α65 for SEAM+PEG(50); see Figure S2), a positive value of the *Y*-axis displacement indicates a shift away from the MT surface, and a positive displacement on the *Z*-axis indicates a shift toward the + end of the MT (see Figure S12 for more details). The PEG(50) heavy atom index is in Table S5, and the direction of the PEG(50) molecules inside both interfaces is in Figure S12. Similar plots for PEG(50)R41 can be found in Figure S13.

Intriguingly, these studies showed that unlike short chain PEG (PEG400), medium and long chain PEGs (such as PEG4700 and PEG20000) possess a high tendency to interact with proteins and even to induce secondary structural changes (unfolding) in the protein. The authors attributed the difference to the presence of a $-CH_2-CH_2-$ hydrophobic group in PEG chains, resulting in an amphiphilic character for the higher MW PEG, versus the purely hydrophilic character of the low MW PEG. Moreover, medium length PEGs (with MW ~ 1000) were particularly capable of forming contacts with proteins through more stable binding sites and stronger interactions.[12] These results prompted us to focus next on the interaction between PEG2000 molecules and lateral interfaces in a MT filament.

Analysis of the MD Simulations of PEG−MT Fragment Complexes Shows That PEGs Do Not Change the Energetics of Lateral Interactions. Analysis of the average backbone RMSD for the MT fragments from our MD simulation runs and of the average RMSD for the MT+PEG complexes (Figure S5) shows that there is little structural fluctuation in the tubulin subunits in the last 10 ns of simulation, when the RMSD reaches a plateau. The PEG (PEG(50)/PEG(50)R41) molecules exhibit higher fluctuations (Figure S6), as expected for a semiflexible polymer in good solvent. Detailed analysis (see section I.1 of the Supporting Information) of the Coulombic and van der Waals interactions between monomers at the lateral interfaces between a full tubulin dimer and its adjacent monomers (Figures S2 and S7) revealed that the presence of the PEG molecules induces only minimal (~1%) changes to the strength of the internal energy compared to the system with water only. Thus, the PEG molecules do not alter the lateral interfaces (see section I.1 for methodology, Figure S7, and Table S3 of the Supporting Information for more data). While fixing the positions of Cα atoms on the periphery of the system (Figure S4) to mimic the presence of the rest of MT filament might reduce energy changes, especially for the van der Waals term, we believe that this reflects the behavior in MTs because tubulin dimers interacting with PEGs would be restricted in their motions by their contacts with adjacent tubulins in the lattice. This point is supported by the results of recent experimental studies, which showed that PEGs (PEG600 and PEG10k) inhibit MT depolymerization.[8]

We analyzed the water molecules located between the central monomers that form the lateral interfaces in the two MT fragments (see description in section I.1 and Figures S2 and S10 of the Supporting Information). We found differences for both interfaces in the presence of PEG2000, but even these are minimal as the average numbers of waters differ by ~10% versus the reference system without the PEG molecule. (Table S4). For the AWAY fragment we also found an ~12% increase in the number of contacts between the dimers that make up the lateral interface covered by PEG(50) and an ~25% increase in the number of contacts between the dimers that make up the lateral interface covered by PEG(50)R41 (see description in section I.1 and Table S4 of the Supporting Information). These newly formed (non-native) contacts are weak energetically as the energetics of the MT fragments is not changing. The number of contacts between the central monomers did not change for the SEAM interface in the presence of the PEG molecules (see Table S4).

To characterize the movement of the PEG molecules with respect to the surface of the two MT fragments, we evaluated the shifts of each heavy atom from the PEG(50) molecule (see Table S5 for atom numbering and section I.1 from the Supporting Information for methodology) along the *X*-, *Y*-, and *Z*-axes in the average structure from the last 2 ns of each production run versus their original positions from docking, as depicted in Figure 5. For the AWAY model, a part of the PEG(50) molecule is moving deeper into the lateral interface between the α45−α46 monomers (atoms with indices 5−75

https://doi.org/10.1021/acs.jpcb.1c01770
J. Phys. Chem. B XXXX, XXX, XXX−XXX

have negative displacements along the *Y*-axis). At the same time, the PEG(50) atoms with indices 80−125 and 135−151 are moving away from the lateral surface (positive displacements along the *Y*-axis). The atoms with indices 40−140 move toward the dimer 45 (negative displacement along the *X*-axis). We also found that the PEG molecules contract during the simulations from an end-to-end distance of 81 Å to 67 Å, which is expected based on the distribution of the end-to-end distances (Figure S8C). The net result is that the PEG(50) molecule gets closer to dimer 45 (see panels A, B, and C in Figure S11A), causing an increase in the contacts between dimers 45 and 46.

In the SEAM model, changes in the position of PEG(50) indicate that part of the PEG chain is moving outside the cavity formed between the four central monomers (positive displacement along the *Y*-axis for the atoms with indices 70−120, which overlaps with the gap between the α27, β27, β52, and α65 monomers), while the end of PEG(50) chain moves inside the cavity. In addition, a part of the PEG(50) molecule is moving away from dimer 27 (positive displacement on the *X*-axis in Figure 5, and panels D, E, and F in Figure S11A). The drift of the PEG molecule from the lateral interface is due to the contraction in its end-to-end distance from 81 to 65 Å, recalling the behavior at the AWAY surface, and to the presence of charged residues on the surface of the SEAM. These changes allow the PEG(50) molecule to fit better inside the defects from the SEAM interface. In summary, our simulations show similar behavior of PEG(50) molecules at both interfaces (AWAY and SEAM), which allows them to fit well within the gaps from these interfaces.

From the analysis of the simulations of PEG(50)R41 and the two MT fragments (Figure S13), we found that PEG(50)R41 has a clear tendency to penetrate deeper into the pores of the lateral interfaces (negative values of *Y*-axis displacement seen in Figure S11B) and to adjust its shape to fit better in the gaps between neighboring tubulin monomers (Figure S11B) rather than to move away from the surface. We note that PEG(50)R41 displays only a minimal contraction in the end-to-end distance: from 41 Å initially to an average of 37 Å, which keeps the end-to-end distance within the most probable region for this PEG length (Figure S8C).

In summary, our studies of the interaction between PEG2000 molecules and the two MT fragments showed the following: (i) PEG does not alter the energetics of the main MT lattice fragments corresponding to the two types of lateral interfaces (A- and B-lattice). (ii) PEG drifts away from charged residues and localizes preferentially in the regions with the largest cavities, such as at the interface between four monomers from two neighboring protofilaments at the SEAM, and PEG(50)R41 in particular tends to get buried in these cavities. This recapitulates the behavior seen in studies of PEGs at other protein quaternary structure interfaces with defects.[22,33] (iii) For the regular lateral interfaces PEG induces the formation of ∼12−25% non-native contacts between the two protofilaments primarily by driving a collapse of their common interface toward the lumen of the MT filament. This latest finding recalls the behavior seen in our previous studies of the indentation of an MT filament with the plus end free, which is the modeling setup that led to an excellent agreement with *in vitro* experimental data on the bending of the filament under the action of a severing protein:[18] early steps in the indentation process correspond to the formation of non-native contacts at lateral interfaces in the filament due to the inward rotation of protofilaments. Thus, to probe the influence that the osmotic pressure due to crowding by PEGs has on MT filaments, we employed a setup inspired by our indentation studies, as described in the Methods section.

Mechanical Response of MT Filaments to an Applied Pressure. *Force Distribution for Compression Using Various Loading Rates Predicts a Low Force Regime for MT Lattice Breaking under Experimental Conditions.* The collapse of MT filaments under pressure, resulting for example from the crowding by osmolytes such as PEG molecules,[3,4] can be modeled through the compression of the filament between two surfaces, where one surface applies a distributed force, ramping up with a vanishingly low loading rate, on the lattice. Because of the extremely long times required for the probing of such action, we instead analyzed the response of a MT filament to distributed forces applied under decreasing loading rates, and we used our results to predict the behavior of the lattice corresponding to the very low loading rates regime.

We focused on the investigation of the mechanical response of a MT lattice to changes in the applied loading rate by probing the action of forces on the three main regions of a 13-protofilament MT filament: the SEAM region (the A-lattice, between protofilaments 1 and 13, P1/P13) and the two interfaces opposite from the seam, called AWAY: the interface directly across from the SEAM (between protofilaments 6 and 7, P6/P7) and the weakest interface in the MT (between protofilaments 5 and 6, P5/P6).[17,18] From our simulations we collected data for the first breaking force (FBF) (see Figure S14), which corresponds to the first break of all the lateral contacts along the length of a tubulin dimer. This force is a good measure for how difficult it is to begin the process of cutting the lattice, as seen during the severing of MTs at the start of mitosis.[17−19,34,35] In our earlier work[17,18] we found that the lattice breaking process is reversible as long as there are no longitudinal cracks inside the protofilaments.

The Big Tip (a cantilever sphere of 100 nm radius, BT) model corresponds to the pushing on a MT by using a flat surface covering the entire length of an eight dimers long MT filament. This setup is very different from the Small Tip (a cantilever sphere of 10 nm radius, ST) model resulting, under normal loading rate conditions (2.000 μm/s) equal to the speed of indentation in AFM experiments,[20] in slightly distinct distributions of the first breaking forces (Figure 6). Namely, the BT model leads to higher forces than the ST model. Importantly, the distribution from the ST model agrees very well with the distribution found in our earlier studies for 8 and 12 dimer long MT filaments (between 270 and 530 pN), which used the ST cantilever and the same loading rate but fixed end MTs.[17,18]

The differences between the distributed (BT) and the concentrated (ST) force setups are visible also upon the decrease of the loading rate: while the FBF values extracted from all the probed models drop with the loading rate, as expected,[36,37] the pattern of force decrease differed substantially between the BT and the ST models (see Figure 7 and Figures S15−S18). Namely, we found that the distribution of the average FBF versus the log of the relative loading rate (LR) for the ST models is fitted very well by a sigmoidal function (Figure 7 and Figure S15), which predicts a leveling off of the force values at both very high and very low loading rates. In contrast, the distribution of the average FBF versus the log of the relative loading rate for the BT models follows an exponential fit, thus leveling off only in the very low loading

https://doi.org/10.1021/acs.jpcb.1c01770
J. Phys. Chem. B XXXX, XXX, XXX−XXX

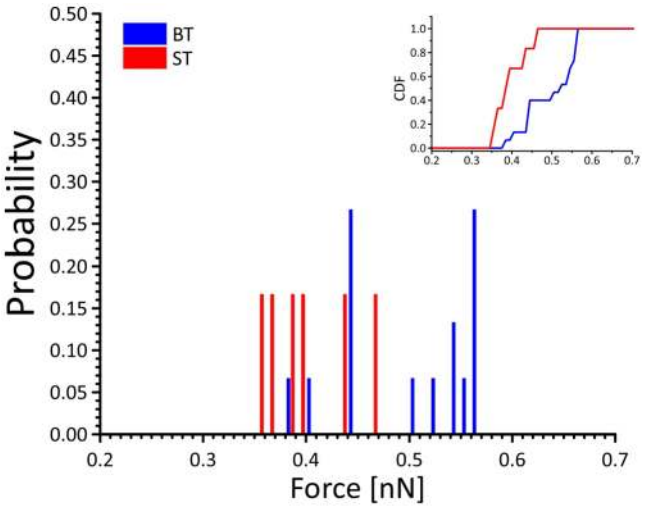

Figure 6. Histograms of FBFs for BT (blue) and ST (red) models at normal (high) loading rate. Right upper corner: inset with the corresponding cumulative distribution functions.

rates regime (see Figure 7 and Figures S16–S18). The plateau at the high loading rates for the ST model suggests that there exists a critical value of the speed of indentation beyond which no increase in the force response (FBF value) of a MT lattice is possible. We attribute this behavior (the force plateau) to the fact that a critical value of the breaking force is reached when the rate of indentation exceeds dramatically the rate of force propagation through the MT lattice. On the other hand, in the case of the almost flat surface (BT model), because the force is distributed throughout the length of the two adjacent protofilaments that will eventually break from one another, the actual force acting on each lateral contact between two tubulin dimers is considerably smaller than the value of the concentrated force from the ST model obtained by using the same loading rate. Thus, the leveling-off of the FBF in the BT case cannot occur until the loading rate reaches higher values than in the ST case. The low loading rate regime gives rise to similar behavior and force values for both the ST and the BT models because, irrespective of the indentation model used, the rise of the force in time is slow enough to allow for the full loading of the lateral contacts in the weakest part of the MT filament that are the first to break. Moreover, these results are compatible only with a model according to which the breaking of the lateral interfaces in a MT filament occurs by unzipping, not shearing. Finally, we note that here, in contrast with our previous studies of indentation for MT lattices with one or two fixed ends,[18] finite-size effects are playing only a minimal role in the force distributions (as seen in the similarity of the distributions from Figures S16–S18 for 8, 6, and, 12 dimers long MTs under BT compression).

Using the extrapolation of the fitting curves for the BT, LT, and the ST models at vanishingly small loading rates, we can predict the minimal forces required for breaking of MTs (see panel B in Figure 7). The models yield similar values of the minimal FBF, leading to an average force of 17.53 ± 14.35 pN. We note that this force regime recalls results from recent experiments,[38] which showed that the ClpB motor applies forces below 50 pN to translocate proteins. Because ClpB and the MT severing proteins katanin and spastin are part of the same AAA+ clade of proteins,[39] the experimentally found low

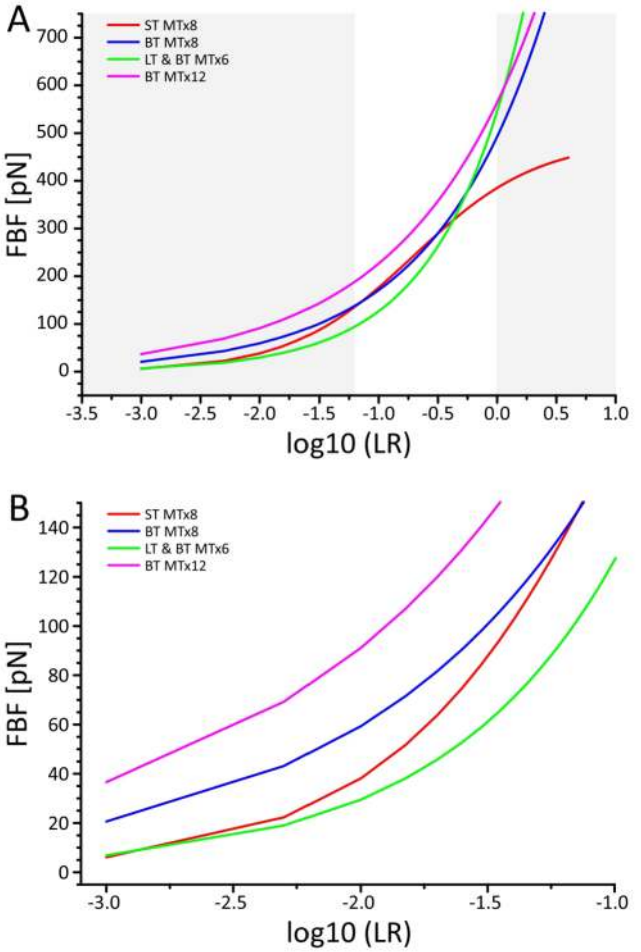

Figure 7. Extrapolation (gray boxes on panel A) of the fitting curves for the FBFs vs log of the relative loading rate (LR) obtained from all our models. Panel A: sigmoidal fitting to all ST models (indentation at P5/P6 and P6/P7) on a MTx8 polymer and exponential fitting to all BT models (indentation at positions P1/P13, P5/P6, and P6/P7) on a MTx8 polymer; LT and BT models on a MTx6 polymer (six dimers long); and all BT models on a MTx12 polymer (12 dimers long). Panel B: magnification of the low loading rates region for all models. Plots with points representing the data from each trajectory are shown in Figures S15–S18.

forces for ClpB lend credence to the forces predicted from our simulations.

Structural Changes in MTs during Compression Show That the Lateral Interfaces Directly in Contact with the Surfaces Break First. For all trajectories corresponding to the compression of a MT under the action of large cantilever tips (BT and LT), we found a similar MT breaking pattern. The first lateral break occurs always in the weakest interface located close to the plate, followed by a break in the weakest interface located below the tip (see Figure S19), which recalls the behavior from our previous studies.[17,18] The reason the interface located right under the tip is strengthened, thus breaking only in a later step, is due to the fact that to adapt to the pressure exerted by the tip of the cantilever sphere, the MT surface needs to change its curvature: under the tip, the MT surface first has to flatten and then to reverse curvature to adjust to the shape of the tip. This leads to the formation of the additional contacts (non-native), thus strengthening the lateral interfaces between protofilaments, as described in our previous

https://doi.org/10.1021/acs.jpcb.1c01770
J. Phys. Chem. B XXXX, XXX, XXX−XXX

Table 1. Average *a* and *b* Lengths of the Minor and Major Axes of the Ellipse Formed by the Cross Section of the MT Filament during Compression[a]

P1/P13		P5/P6		P6/P7	
a (nm)	*b* (nm)	*a* (nm)	*b* (nm)	*a* (nm)	*b* (nm)
21.10 ± 1.02	32.49 ± 0.59	21.52 ± 1.80	32.09 ± 1.17	20.37 ± 1.73	32.21 ± 1.12

[a]The values are measured at the FBF event for the MTx8 BT system and averaged over all trajectories for a given setup.

work.[18] The number of non-native contacts drops to zero right when the first break occurs. We found that the rate of increase in non-native contacts slows down with the reduction of the LR. On the opposite side of the MT close to the plate, for all lateral interfaces in our models we found an increase in the non-native contacts, which differs from the one below the tip: after an initial increase, the number of non-native contacts remains stable. This is followed, very often before the break, by a rapid increase and then their reduction to zero right after the break (see Figure S20).

Our findings agree with the results of recent experimental studies, which showed that the lateral interactions between protofilaments are the most sensitive to the external pressure.[3] We also characterized the deformation of the circular cross section of the MTx8 lattice under BT compression conditions. We found (Table 1) that the cross section becomes elliptical at the point of the first break (FBF) event, as depicted in Figure 8, with average lengths of the minor and major axes at 20 and

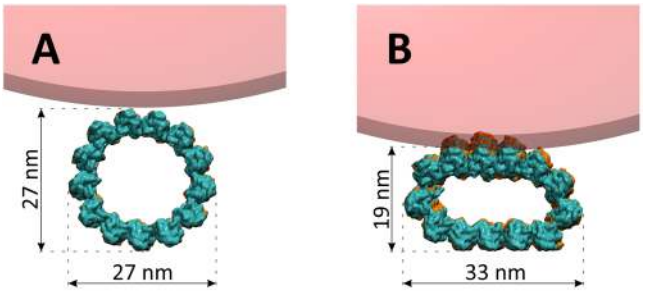

Figure 8. Example snapshots of the cross section (after the fourth ring, view from the + side) of the MT from the MTx8 BT P6/P7 model with LR 2.000 μm/s at the starting point (A) and at the FBF event (B). Orange/cyan surfaces are representations of α/β-tubulin monomers; red transparent sphere: indentation tip. The lower plate has been omitted for clarity.

32 nm, respectively. These values are strikingly close to the lattice parameters of ∼19 and 33 nm found in the rectangular lattice arrangement of MT bundles formed due to the crowding of MTs by 20k PEOs.[4,5] Details of the pathways for each of the three BT setups and for the ST simulations are provided below.

BT Compression between P1/P13 (SEAM). When the external force is applied on the seam of the MT filament by using the surface (BT) setup, we found that the first lateral crack occurs on the weakest interface (P5/P6) located close to the plate (for the strength of the lateral interfaces see Figure S21). This is followed by a lateral crack on the P7/P8 and the P6/P7 interfaces, all located close to the plate, and then the interface located right under the tip (the P1/P13 interface) and the P9/P10 interface break (Figure S19).

BT Compression between P5/P6 (Weakest Interface). When the external force is applied to the weakest lateral interface (P5/P6) of the MT filament by using the surface (BT) setup, the first lateral crack occurs at the SEAM (P1/P13 interface), which is located above the plate. This is followed by a crack on the P11/P12 interface, which is close to the plate, and only afterward by the breaking of the interface located right under the tip (the P5/P6 interface). Finally, the P9/P10 interface, which is on the side of the MT (Figure S19), breaks. This behavior is consistent for all trajectories and all relative loading rates, and the loss of contacts occurs by slow unzipping. Importantly, we found that the initial breaking event on the P1/P13 interface occurs close to equilibrium: the interface can recover from the first break in the time it takes for the other lateral interfaces to start breaking. Once all the other three interfaces show cracks, the seam finally rips apart rapidly along the length of the protofilament.

BT Compression between P6/P7 (Directly Opposite to the SEAM). When the external force is applied to the lateral interface located directly opposite to the seam (P6/P7) by using the surface (BT) setup, the first lateral crack occurs at the SEAM (P1/P13), which is now directly above the plate (Figure S19). Next, the P5/P6 interface, which is just on the side of the interface on which tip is pushing, cracks, followed by a break of the P9/P10 interface (only for a loading rate of 2.000 μm/s) and then of the P11/P12 interface. Notably, the P6/P7 interface on which we push directly does not break as part of the first set of events.

ST Indentation. For the indentation on the P5/P6 interface at high loading rates (2.000 μm/s) using the ST setup, we found a different pattern than the one seen in the BT setup. The first break occurs right on the pushed interface (P5/P6), followed by the break of the SEAM (P1/P13) and the P11/P12 interfaces, both located close to the plate. For the 1.000 μm/s loading rate, the first break for the majority of the runs (67%) still occurs on the P5/P6 interface, but in 33% of the cases, the SEAM breaks first. The reduction of the loading rate to 0.500 μm/s results in a first break under the tip (P5/P6), followed by the breaking of the SEAM (P1/P13) in 33% of the runs and by the breaking of the P11/P12 interface in the rest of the runs. From this point on, further reductions in the loading rates result in a dramatic change in the breaking pattern of the MT lattice, resulting in the set of steps found for the BT models: the first break no longer occurs under the tip but rather at the SEAM. The next steps correspond to the break of the P5/P6 interface and of the P11/P12 interface. For the indentation on the P6/P7 interface, we found a consistent breaking pattern for all loading rates, which agrees with the pattern for the BT model. The first crack occurs on the SEAM, which is located right above the plate, followed by the break of the P5/P6 interface, which is located close to the tip. The only exception to this behavior is in a single trajectory for the 2.000 μm/s loading rate, where P5/P6 breaks before the SEAM. Upon lowering the loading rate, the break of the P5/P6 interface gets delayed more and more compared to the time of the initial break (of the SEAM). Importantly, our simulations show that the first breaking force is directly proportional to the overall strength of the interfaces in all the models. For example,

https://doi.org/10.1021/acs.jpcb.1c01770
J. Phys. Chem. B XXXX, XXX, XXX−XXX

this is seen when changing the position of the indentation point (see Figures S19 and S20): when a weaker interface is located directly under the tip or above the plate, then this interface breaks first, and it determines the value of the FBF. A similar dependence has been found in other large biomolecular assemblies. For example, for virus capsids[40] the strength of the capsid is related to the mean coordination number and the strength of the native contacts in its structure. Moreover, in accord with these studies, in our simulations, which employ molecular-level descriptions of the protein chains, we found that more of the deformation in the MT filament is concentrated under the tip and at the bottom of the lattice, which is in contact with the plate. In contrast, the sides of the filament are deformed less and thus show less radial expansion than what is assumed in the continuum models used to interpret the behavior of MTs under pressure.[5]

External Pressure. Using the first breaking force data for the BT model, we estimated the external pressure needed to generate cracks in the surface of the MTs. The area for the pressure calculations was the surface of the four PFs under the tip (~72 nm long, over the whole length of the eight dimers long MT, amounting to a total area of 1430 nm^2). The plot of the pressure data vs indentation speed fitted to the one-phase association equation from Figure 9 shows that the maximum

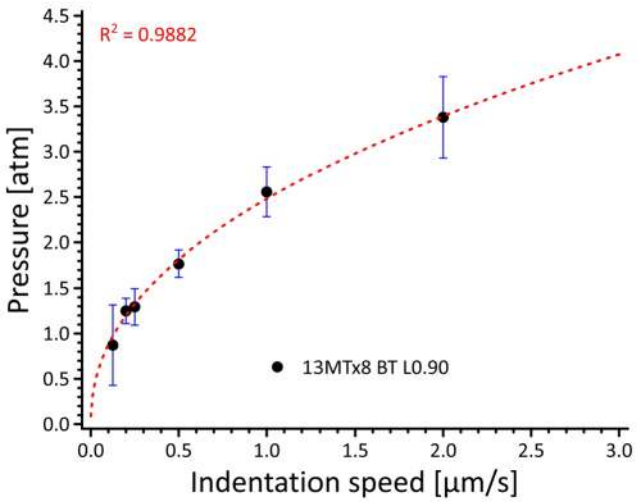

Figure 9. Pressure corresponding to the FBF event vs indentation speed for 13MTx8 in all BT models. Blue lines indicate the standard deviation for each point. The red dashed line is a fitting curve. The R^2 value is in the left top corner.

external pressure necessary to break the surface of MTs is ~4 atm for the compression between two surfaces. At the lower end, the pressure corresponding to our extrapolated minimal FBF is ~7000 Pa. Interestingly, this value is only an order of magnitude higher than the pressure at which the rectangular phase of compressed MT bundles starts to form due to the crowding with 0.4% 20k PEO,[4,5] and it is well within the interval between 600 and 25000 Pa where the rectangular phase of the MT bundle is found.

CONCLUSIONS

Our study shows that PEG molecules at low concentrations and in configurations corresponding to the long tail end of their end-to-end distribution[26] organize water molecules at lateral interfaces between protofilaments, while not changing directly the energetics of the interfaces. Second, that PEG molecules in configurations corresponding to their most probable end-to-end distance target voids or packing defects in MTs, such as the pores from lateral interfaces or the from the seam interface. The penetration of PEGs into these voids during our MD simulations induced the rotation of the two protofilaments forming the lateral interface toward the lumen of the MT filament, leading to the formation of non-native contacts between them. The breaking of MT lattices with ends free, under compression mimicking high crowdedness conditions due to osmolytes such as PEGs, shows that the first event is the loss of lateral interfaces, whose number and identity change with the loading rate. This leads to a change in the cross section of the MT cylinder from a circle to an ellipse, whose axes lengths match experimental values.[4,5] A crucial finding from these simulations is that at the vanishingly low loading rate regime of force application corresponding to experiments the predicted pressure is well within the experimental range.[4,5] Importantly, our previous investigations into the breaking of MTs under the action of mechanical forces showed that the lattice can fully recover after lateral interfaces breaking if the applied pressure is lifted.[16−18] Finally, in accord with the findings of studies of the mechanical response in other large biomolecular assemblies,[40] we did not observe the buckling of lattice under external stress. Thus, our simulations results suggest that the formation of the collapsed MTs with elliptical cross section[4,5] under high crowding by PEGs is the result of the break of lateral interfaces, rather than just buckling of the filament. In accord with investigations into the mechanical response of other large biomolecular assemblies such as viral capsids under different geometries of force application that we and other groups performed,[37,40,41] we found that MTs break more readily under concentrated forces compared to distributed forces. The reason is that when the MT is indented by a distributed force (BT conditions), all the residues in the tip−MT contact area move in the same direction. In contrast, when the MT is indented by a smaller tip (ST conditions), different residues will be pushed in different directions, as seen in the case of virus capsids.[41] Because the ST conditions correspond to a smaller contact area between the tip and the MT surface, they lead to a weaker mechanical response (lower breaking force). However, here we show that this behavior is highly dependent on the loading rate, as differences between these two extreme ways of force action vanish in the low loading rate regime, which is the relevant force (pressure) regime for *in vitro* experiments and cellular conditions. Furthermore, we observed that the main influence on the value of the FBFs is the number and the strength of the native contacts that are broken during trajectories, recalling the results for virus capsids.[37] These findings are important for example in understanding the action of severing proteins, which take apart the MT lattice and are believed to work in tandem as we and others showed.[19,34,42]

ASSOCIATED CONTENT

Supporting Information

The Supporting Information is available free of charge at https://pubs.acs.org/doi/10.1021/acs.jpcb.1c01770.

Supplemental data analysis; Table S1, list of MD simulations for MT fragments with and without PEG2000 molecules; Table S2, number of trajectories for the compression studies of each MT system; Table

https://doi.org/10.1021/acs.jpcb.1c01770
J. Phys. Chem. B XXXX, XXX, XXX−XXX

S3, average energies from MD simulations; Table S4, average number of contacts and water molecules from MD simulations; Table S5, list heavy atoms in PEG molecules; Figure S1, schematics of an MT filament with 13 protofilaments and 8 dimers in length; Figure S2, cartoon of the position of monomers for the AWAY and SEAM models; Figure S3, cartoon representation for the AWAY system with docking gird points; Figure S4, representation of the AWAY reference system for the MD simulation runs; Figure S5, average MT backbone RMSD plots from all production runs; Figure S6, RMSD plots for all heavy atoms from PEG molecules from MD production runs; Figure S7, energy plots for the last 10 ns of the MD production runs for the central dimers; Figure S8, normalized distribution of the end-to-end distances for PEGs; Figure S9, docking of PEG molecules on the AWAY and SEAM interfaces; Figure S10, water molecules located close to the central dimer; Figure S11, comparison of initial position of PEG2000 molecules vs their position in the average structure from the last 2 ns of production runs; Figure S12, schematics of the PEG(50) position analysis; Figure S13, change in the position of the heavy atoms of the three PEG(50)-R41 molecules in the MD runs; Figure S14, example of force vs frame and force vs depth for compression runs; Figure S15, FBFs vs log of LR for the ST models; Figure S16, FBFs vs log of LR for BT models; Figure S17, FBFs vs log of LR for LT models; Figure S18, FBFs vs log of LR for the 12 dimers long MT with BT model; Figure S19, schematics showing the relative position of interfaces in MT filament; Figure S20, example of RQn plots for 13MTx8 P1/P13 compression using the BT setup; Figure S21, list of the total number of native contacts and energy per lateral interface (PDF)

AUTHOR INFORMATION

Corresponding Author

Ruxandra I. Dima − *Department of Chemistry, University of Cincinnati, Cincinnati, Ohio 45221, United States;* orcid.org/0000-0001-6105-7287; Phone: +1 (513) 556-3961; Email: ruxandra.dima@uc.edu; Fax: +1 (513) 556-9239

Authors

Lukasz Szatkowski − *Department of Chemistry, University of Cincinnati, Cincinnati, Ohio 45221, United States; Division of Science, Mathematics, and Engineering, University of South Carolina Sumter, Sumter, South Carolina 29150, United States*

Rohith Anand Varikoti − *Department of Chemistry, University of Cincinnati, Cincinnati, Ohio 45221, United States*

Complete contact information is available at: https://pubs.acs.org/10.1021/acs.jpcb.1c01770

Notes

The authors declare no competing financial interest.

ACKNOWLEDGMENTS

This work was supported in part by a grant from the National Science Foundation: MCB-18179488 (to R.I.D.). R.I.D. thanks Prof. Dave Thirumalai for serving as a role model in developing her scientific career. L.S. thanks Research Computing at the University of South Carolina for access to the Hyperion High Performance Cluster. The authors thank Prof. Richard Sessions from the University of Bristol for access to the BUDE software.

REFERENCES

(1) Minton, A. P. How Can Biochemical Reactions Within Cells Differ From Those in Test Tubes? *J. Cell Sci.* **2006**, *119*, 2863−2869.

(2) Conway, L.; Wood, D.; Tüzel, E.; Ross, J. L. Motor Transport of Self-Assembled Cargos in Crowded Environments. *Proc. Natl. Acad. Sci. U. S. A.* **2012**, *109*, 20814−20819.

(3) Gao, M.; Berghaus, M.; Möbitz, S.; Schuabb, V.; Erwin, N.; Herzog, M.; Julius, K.; Sternemann, C.; Winter, R. On the Origin of Microtubules' High-Pressure Sensitivity. *Biophys. J.* **2018**, *114*, 1080−1090.

(4) Needleman, D. J.; Ojeda-Lopez, M. A.; Raviv, U.; Ewert, K.; Jones, J. B.; Miller, H. P.; Wilson, L.; Safinya, C. R. Synchrotron X-Ray Diffraction Study of Microtubules Buckling and Bundling Under Osmotic Stress: A Probe of Interprotofilament Interactions. *Phys. Rev. Lett.* **2004**, *93*, 198104.

(5) Needleman, D. J.; Ojeda-Lopez, M. A.; Raviv, U.; Ewert, K.; Miller, H. P.; Wilson, L.; Safinya, C. R. Radial Compression of Microtubules and the Mechanism of Action of Taxol and Associated Proteins. *Biophys. J.* **2005**, *89*, 3410−3423.

(6) Chung, P. J.; Song, C.; Deek, J.; Miller, H. P.; Li, Y.; Choi, M. C.; Wilson, L.; Feinstein, S. C.; Safinya, C. R. Comparison Between 102k and 20k Poly (Ethylene Oxide) Depletants in Osmotic Pressure Measurements of Interfilament Forces in Cytoskeletal Systems. *ACS Macro Lett.* **2018**, *7*, 228−232.

(7) Hilitski, F.; Ward, A. R.; Cajamarca, L.; Hagan, M. F.; Grason, G. M.; Dogic, Z. Measuring Cohesion Between Macromolecular Filaments One Pair at a Time: Depletion-Induced Microtubule Bundling. *Phys. Rev. Lett.* **2015**, *114*, 138102.

(8) Bachand, G. D.; Jain, R.; Ko, R.; Bouxsein, N. F.; VanDelinder, V. Inhibition of Microtubule Depolymerization by Osmolytes. *Biomacromolecules* **2018**, *19*, 2401−2408.

(9) Leibler, S.; Singh, R. R.; Fisher, M. E. Thermodynamic Behavior of Two-Dimensional Vesicles. *Phys. Rev. Lett.* **1987**, *59*, 1989.

(10) Seifert, U. Adhesion of Vesicles in Two Dimensions. *Phys. Rev. A: At., Mol., Opt. Phys.* **1991**, *43*, 6803.

(11) Memet, E.; Hilitski, F.; Morris, M. A.; Schwenger, W. J.; Dogic, Z.; Mahadevan, L. Microtubules Soften Due to Cross-Sectional Flattening. *eLife* **2018**, *7*, e34695.

(12) Wu, J.; Zhao, C.; Lin, W.; Hu, R.; Wang, Q.; Chen, H.; Li, L.; Chen, S.; Zheng, J. Binding Characteristics Between Polyethylene Glycol (PEG) and Proteins in Aqueous Solution. *J. Mater. Chem. B* **2014**, *2*, 2983−2992.

(13) Brogan, A. P.; Sessions, R. B.; Perriman, A. W.; Mann, S. Molecular Dynamics Simulations Reveal a Dielectric-Responsive Coronal Structure in Protein-Polymer Surfactant Hybrid Nano-constructs. *J. Am. Chem. Soc.* **2014**, *136*, 16824−16831.

(14) Pérez, B.; Coletta, A.; Pedersen, J. N.; Petersen, S. V.; Periole, X.; Pedersen, J. S.; Sessions, R. B.; Guo, Z.; Perriman, A.; Schiøtt, B. Insight Into the Molecular Mechanism Behind Peg-Mediated Stabilization of Biofluid Lipases. *Sci. Rep.* **2018**, *8*, 1−13.

(15) Sousa, S. F.; Peres, J.; Coelho, M.; Vieira, T. F. Analyzing PEGylation Through Molecular Dynamics Simulations. *ChemistrySelect* **2018**, *3*, 8415−8427.

(16) Kononova, O.; Kholodov, Y.; Theisen, K. E.; Marx, K. A.; Dima, R. I.; Ataullakhanov, F. I.; Grishchuk, E. L.; Barsegov, V. Tubulin Bond Energies and Microtubule Biomechanics Determined From Nanoindentation *In Silico*. *J. Am. Chem. Soc.* **2014**, *136*, 17036−17045.

(17) Jiang, N.; Bailey, M. E.; Burke, J.; Ross, J. L.; Dima, R. I. Modeling the Effects of Lattice Defects on Microtubule Breaking and Healing. *Cytoskeleton* **2017**, *74*, 3−17.

(18) Szatkowski, L.; Merz, D. R., Jr.; Jiang, N.; Ejikeme, I.; Belonogov, L.; Ross, J. L.; Dima, R. I. Mechanics of the Microtubule Seam Interface Probed by Molecular Simulations and *In Vitro* Severing Experiments. *J. Phys. Chem. B* **2019**, *123*, 4888−4900.
(19) Varikoti, R. A.; Macke, A. C.; Speck, V.; Ross, J. L.; Dima, R. I. Molecular Investigations Into the Unfoldase Action of Severing Enzymes on Microtubules. *Cytoskeleton* **2020**, *77*, 214−228.
(20) de Pablo, P. J.; Schaap, I. A.; MacKintosh, F. C.; Schmidt, C. F. Deformation and Collapse of Microtubules on the Nanometer Scale. *Phys. Rev. Lett.* **2003**, *91*, 098101.
(21) Schaap, I. A.; De Pablo, P. J.; Schmidt, C. F. Resolving the Molecular Structure of Microtubules Under Physiological Conditions with Scanning Force Microscopy. *Eur. Biophys. J.* **2004**, *33*, 462−467.
(22) Settanni, G.; Zhou, J.; Suo, T.; Schöttler, S.; Landfester, K.; Schmid, F.; Mailänder, V. Protein Corona Composition of Poly (Ethylene Glycol)-and Poly (Phosphoester)-Coated Nanoparticles Correlates Strongly With the Amino Acid Composition of the Protein Surface. *Nanoscale* **2017**, *9*, 2138−2144.
(23) Hyeon, C.; Dima, R. I.; Thirumalai, D. Pathways and Kinetic Barriers in Mechanical Unfolding and Refolding of RNA and Proteins. *Structure* **2006**, *14*, 1633−1645.
(24) Tanner, D. E.; Chan, K.-Y.; Phillips, J. C.; Schulten, K. Parallel Generalized Born Implicit Solvent Calculations with NAMD. *J. Chem. Theory Comput.* **2011**, *7*, 3635−3642.
(25) Phillips, J. C.; Hardy, D. J.; Maia, J. D.; Stone, J. E.; Ribeiro, J. V.; Bernardi, R. C.; Buch, R.; Fiorin, G.; Hénin, J.; Jiang, W.; et al. Scalable Molecular Dynamics on CPU and GPU Architectures with NAMD. *J. Chem. Phys.* **2020**, *153*, 044130.
(26) Sherck, N.; Webber, T.; Brown, D. R.; Keller, T.; Barry, M.; DeStefano, A.; Jiao, S.; Segalman, R. A.; Fredrickson, G. H.; Shell, M. S.; et al. End-to-End Distance Probability Distributions of Dilute Poly (ethylene oxide) in Aqueous Solution. *J. Am. Chem. Soc.* **2020**, *142*, 19631−19641.
(27) McIntosh-Smith, S.; Price, J.; Sessions, R. B.; Ibarra, A. A. High Performance In Silico Virtual Drug Screening on Many-Core Processors. *Int. J. High Perform. Comput. Appl.* **2015**, *29*, 119−134.
(28) Humphrey, W.; Dalke, A.; Schulten, K. VMD: Visual Molecular Dynamics. *J. Mol. Graphics* **1996**, *14*, 33−38.
(29) Zhmurov, A.; Dima, R.; Kholodov, Y.; Barsegov, V. Sop-GPU: Accelerating Biomolecular Simulations in the Centisecond Timescale Using Graphics Processors. *Proteins: Struct., Funct., Genet.* **2010**, *78*, 2984−2999.
(30) Roll-Mecak, A.; Vale, R. D. Structural Basis of Microtubule Severing by the Hereditary Spastic Paraplegia Protein Spastin. *Nature* **2008**, *451*, 363−367.
(31) Devanand, K.; Selser, J. Asymptotic Behavior and Long-Range Interactions in Aqueous Solutions of Poly (Ethylene Oxide). *Macromolecules* **1991**, *24*, 5943−5947.
(32) Svergun, D. I.; Ekström, F.; Vandegriff, K. D.; Malavalli, A.; Baker, D. A.; Nilsson, C.; Winslow, R. M. Solution Structure of Poly (Ethylene) Glycol-Conjugated Hemoglobin Revealed by Small-Angle X-Ray Scattering: Implications for a New Oxygen Therapeutic. *Biophys. J.* **2008**, *94*, 173−181.
(33) Prabhakaran, M.; Manjula, B. N.; Acharya, S. A. Molecular Modeling Studies of Surface Decoration of Hemoglobin by Maleimide PEG. *Artif. Cells Nanomed. Biotechnol.* **2006**, *34*, 381−393.
(34) Vemu, A.; Szczesna, E.; Zehr, E. A.; Spector, J. O.; Grigorieff, N.; Deaconescu, A. M.; Roll-Mecak, A. Severing Enzymes Amplify Microtubule Arrays Through Lattice GTP-Tubulin Incorporation. *Science* **2018**, *361*, eaau1504.
(35) McNally, F. J.; Roll-Mecak, A. Microtubule-Severing Enzymes: From Cellular Functions to Molecular Mechanism. *J. Cell Biol.* **2018**, *217*, 4057−4069.
(36) Bell, G. I. Models for the Specific Adhesion of Cells to Cells. *Science* **1978**, *200*, 618−627.
(37) Cieplak, M.; Robbins, M. O. Nanoindentation of Virus Capsids in a Molecular Model. *J. Chem. Phys.* **2010**, *132*, 015101.
(38) Avellaneda, M. J.; Franke, K. B.; Sunderlikova, V.; Bukau, B.; Mogk, A.; Tans, S. J. Processive Extrusion of Polypeptide Loops by a Hsp100 Disaggregase. *Nature* **2020**, *578*, 317−320.
(39) Dima, R. I; Stan, G. In *Computational Studies of Mechanical Remodeling of Substrate Proteins by AAA+ Biological Nanomachines*; Tonelli, A. E., Patterson, G., Eds.; ACS Symp. Ser. "Modern Applications of Flory's Statistical Mechanics of Chain Molecules"; American Chemical Society: 2020; pp 117−141.
(40) Cieplak, M.; Robbins, M. O. Nanoindentation of 35 Virus Capsids in a Molecular Model: Relating Mechanical Properties to Structure. *PLoS One* **2013**, *8*, e63640.
(41) Kononova, O.; Snijder, J.; Brasch, M.; Cornelissen, J.; Dima, R. I.; Marx, K. A.; Wuite, G. J.; Roos, W. H.; Barsegov, V. Structural Transitions and Energy Landscape for Cowpea Chlorotic Mottle Virus Capsid Mechanics From Nanomanipulation *In Vitro* and *In Silico*. *Biophys. J.* **2013**, *105*, 1893−1903.
(42) Sharp, D. J.; Ross, J. L. Microtubule-Severing Enzymes at the Cutting Edge. *J. Cell Sci.* **2012**, *125*, 2561−2569.

https://doi.org/10.1021/acs.jpcb.1c01770
J. Phys. Chem. B XXXX, XXX, XXX−XXX